
Two Calls, Two Moments, and the Vote-Accuracy Curve of Repeated LLM Inference

Yi Liu
York University

Abstract

Repeated sampling is a standard way to spend test-time compute, but its benefit is controlled by the latent distribution of correctness across examples, not by one-call accuracy alone. We study the binary correctness layer of repeated LLM inference under conditional-i.i.d. calls. One labeled call identifies the mean latent success probability; two labeled calls identify its second moment and hence the same-example correctness correlation that separates stable errors from recoverable call-level randomness. From these two moments, every fixed majority-vote budget has a sharp distribution-free two-call interval. The key technical reduction is that the infinite-dimensional moment problem has three-atom extremizers and quadratic dual certificates for every finite budget, so the bounds are exact rather than discretized or parametric. The first useful budget, three votes, has a closed form, width at most $1/8$, and a certified-improvement criterion. The infinite-vote endpoint is the limit of majority voting as the number of calls tends to infinity; it is also sharply bounded, but remains threshold-sensitive because it depends on latent mass around $q = 1/2$. We add maximum-entropy and Latent-difficulty Gaussian-probit point completions, and experiments on LLM calls over QNLI and QQP show that empirical three- and five-vote accuracies are contained in the projected two-call regions while temperature changes and randomized model mixtures can create voting gains not ordered by one-call accuracy.

1 Introduction

Repeated sampling has become a standard way to spend test-time compute. Self-consistency samples multiple reasoning paths before aggregating final answers [25]; $\text{pass}@k$ evaluation measures success across repeated code-generation attempts [6]; and inference-scaling work studies repeated candidate generation as a performance axis [5]. A parallel line uses consistency and entropy of repeated generations as uncertainty evidence, including semantic uncertainty and semantic entropy for hallucination detection and confidence assessment [7, 11, 13]. These methods are especially visible in LLMs, but they leave a basic statistical question open: after fixing a model, prompt, sampler, and parser, how much extra correctness can majority voting extract from more calls?

The difficulty is that consistency is not correctness. Repeated calls may agree because the system reliably solves an example, or because it reliably makes the same mistake. Conversely, a lower-accuracy one-call policy may retain conditional randomness that voting can average away. Thus repeated-inference planning needs a statistic of *votability*: the extent to which same-example calls still contain independent correctness information after conditioning on the example. This statistic is not determined by one-call accuracy.

We isolate the binary correctness layer. Each call is reduced to a correctness bit. On an example with latent success probability q , a strict majority of $2n + 1$ conditionally independent calls succeeds with probability $P_n(q) = \Pr\{\text{Bin}(2n + 1, q) \geq n + 1\}$. Even vote budgets add no new accuracies under symmetric tie-breaking, because a fair-tie $2n$ -vote rule has the same success probability as the

preceding $(2n - 1)$ -vote rule (Appendix A.1). If Q is the population law of example-level success probabilities, the distinct vote-accuracy curve is $V_n = \mathbb{E}P_n(Q)$ for $n = 0, 1, 2, \dots$. This curve is the operational object: it says whether three, five, or more calls improve on one.

Estimating the full latent law of Q seems to require many repeated labeled calls per example. Our main point is that this is too pessimistic for finite-vote certification from two calls. One labeled call identifies only $\mu = \mathbb{E}Q$. A second labeled call identifies $\nu = \mathbb{E}Q^2$, equivalently the same-example correctness correlation $\rho = (\nu - \mu^2)/\{\mu(1 - \mu)\}$. The pair table from two calls tells how often two calls are both correct, both wrong, or disagree. It therefore converts a potentially many-call validation problem into a two-call moment problem: the full curve is not identified, but the vote-relevant ambiguity is sharply delimited.

The central reduction is that this two-moment ambiguity class is computationally tractable without imposing a latent parametric model. For every fixed finite vote budget, optimizing over all laws on $[0, 1]$ with moments (μ, ν) reduces to a three-atom problem and an equivalent quadratic dual certificate. The same three-atom geometry applies to any polynomial objective in the latent probability q , so it can certify not only V_n itself but also derived planning quantities such as the largest possible additional gain $V_3 - V_1$. We use this reduction to obtain sharp endpoints for all finite budgets, a closed-form three-vote case, and a separate analysis of the infinite-vote endpoint. The endpoint is the limit of V_n as the number of votes grows, so it equals the latent mass above the threshold $q = 1/2$ plus half the mass exactly at the threshold; unlike finite budgets, it is threshold-sensitive rather than polynomial.

Two moments also support useful point completions when a single curve is desired. The maximum-entropy completion is the least-informative law on $[0, 1]$ with the observed moments, the bounded-support analogue of the Gaussian maximum-entropy principle. Latent-difficulty Gaussian-probit (LDGP) uses the established normal-ogive/probit item-response difficulty model for binary correctness; after scale normalization it has exactly two free parameters, so the same two-call moments identify an entire LDGP vote curve. These completions are summaries, not substitutes for the nonparametric identified intervals.

The experiments use GLUE QNLI and QQP [24] with three local model families, three temperatures, and five repeated calls per example. Across 18 policy-dataset pairs, empirical three- and five-vote accuracies are contained in the projected two-call regions. The same data show why one-call accuracy is not an ordering for repeated inference: high-correlation policies may gain almost nothing from voting, while lower-correlation policies and randomized model mixtures can overtake higher one-call baselines after voting.

1.1 Contributions

- We formulate repeated LLM correctness through a latent example-level success probability Q and show that two labeled calls identify the pair table, the two-moment class (μ, ν) , and the same-example correctness correlation that separates stable errors from recoverable randomness.
- We prove sharp distribution-free two-call certificates for every finite majority-vote budget. The key reduction is that the infinite-dimensional ambiguity class can be optimized over a three-atom space, with matching quadratic dual certificates; the same reduction applies to polynomial objectives such as marginal vote gains.
- We derive the closed-form three-vote interval and certified-improvement criterion, characterize the infinite-vote endpoint, add MaxEnt and LDGP point completions, and validate the resulting regions on repeated LLM inference with temperature changes, mixtures, and overtaking examples.

2 Related work

Repeated sampling and test-time scaling. Self-consistency decoding made repeated reasoning-path sampling a central empirical tool for LLM reasoning [25]. Adaptive and confidence-aware variants spend samples selectively [1, 22]. Code-generation work measures repeated attempts through $\text{pass}@k$ [6], and inference-scaling studies investigate repeated sampling over much larger budgets [5]. These papers motivate repeated inference planning, but $\text{pass}@k$ is an at-least-one-success criterion and semantic or plurality self-consistency depends on how wrong answers split across alternatives.

Here the target is binary majority-vote certification from one or two labeled calls, without assuming a full latent law.

Agreement, uncertainty, and repeated prompts. Agreement and semantic clustering are widely used as uncertainty signals. SelfCheckGPT compares sampled outputs for hallucination detection [13]; semantic entropy accounts for linguistic equivalence of answers [7, 11]; and later uncertainty benchmarks and conformal variants study calibration and coverage [21, 23, 26, 28]. LLM outputs may vary even in nominally deterministic settings [3], and treating repeated prompts as independent examples can overstate effective sample size [8, 14]. Our binary correctness layer separates agreement from correctness: two labeled calls estimate the first two moments of the latent correctness distribution and the same-example correlation that determines whether repeated calls add independent evidence.

Moment geometry. The sharp envelopes below are finite moment problems. Extreme points of moment sets have small support [19, 27], and quadratic majorants/minorants give dual certificates closely related to optimal probability inequalities [4, 10]. The maximum-entropy completion follows Jaynes’ principle of choosing the least-committal distribution under known constraints [9]; in this problem it becomes a two-parameter quadratic-exponential density on $[0, 1]$. The LDGP completion uses the normal-ogive/probit item-response view of binary correctness [2, 12].

3 Repeated-call model

We now fix the notation used throughout the paper. Let $Y_i \in \{-1, +1\}$ be the ground-truth label and let \widehat{Y}_{ij} be the output of repeated call j on example i . Let π be the population law of latent within-example success probabilities, and let $Q \sim \pi$ denote a generic draw. For each example, define

$$B_{ij} = \mathbf{1}\{\widehat{Y}_{ij} = Y_i\}, \quad q_i \stackrel{\text{i.i.d.}}{\sim} \pi, \quad B_{ij} \mid q_i \stackrel{\text{ind}}{\sim} \text{Bernoulli}(q_i). \quad (1)$$

Here q_i is the within-example success probability for example i , while Q is a generic latent success probability drawn from the same across-example law. The pair (B_{i1}, B_{i2}) is the noisy two-call observation from that example. Repeated calls are dependent after marginalizing over examples, but independent after conditioning on q_i .

Shared protocol components change the induced law π rather than the logic of (1). A fixed prompt template, fixed system prompt, model choice, temperature, and output parser are part of the protocol. Conditional independence requires fresh remaining randomness across calls after conditioning on q_i ; hidden serving-state reuse, adaptive prompting after earlier calls, or correlated decoding streams would require a richer latent state. At the sampling level, the independent units are examples, not calls.

Scope of the binary layer. The theory concerns correctness bits and strict majority over those bits. Pass@ k asks for at least one success, semantic or plurality self-consistency depends on the allocation of wrong answers, and verifier- or prompt-adaptive schemes change the latent state. These settings can motivate repeated inference but are not scalar- Q majority-vote problems without additional structure.

Odd budgets follow from the voting rule rather than an artificial restriction. With symmetric tie-breaking, an even vote has the same success probability as the preceding odd vote. Indeed, if

$$P_n^{\text{even}}(q) = \mathbb{P}\{\text{Bin}(2n, q) > n\} + \frac{1}{2}\mathbb{P}\{\text{Bin}(2n, q) = n\},$$

then $P_n^{\text{even}}(q) = P_{n-1}(q)$ for every q . Thus a fair-tie $2n$ -vote rule equals a $(2n - 1)$ -vote rule in accuracy, and it suffices to index the distinct majority-vote accuracies by odd representatives.

For the representative budget $2n + 1$, define

$$P_n(q) = \sum_{\ell=n+1}^{2n+1} \binom{2n+1}{\ell} q^\ell (1-q)^{2n+1-\ell}, \quad V_n(\pi) = \int P_n(q) d\pi(q), \quad (2)$$

with π as above. The one-call accuracy is $V_0 = \mu = \mathbb{E}Q$.

The infinite-vote endpoint is not a new voting rule; it is the limit of the same majority rule as the number of conditionally independent calls goes to infinity. For fixed q , the binomial law of large numbers gives $P_n(q) \rightarrow 1$ when $q > 1/2$ and $P_n(q) \rightarrow 0$ when $q < 1/2$. At $q = 1/2$, odd-majority symmetry gives $P_n(1/2) = 1/2$ for every n . Hence bounded convergence gives

$$V_\infty(\pi) := \lim_{n \rightarrow \infty} V_n(\pi) = \pi((1/2, 1]) + \frac{1}{2}\pi(\{1/2\}). \quad (3)$$

This threshold form explains the endpoint sensitivity: tiny shifts of latent mass around $q = 1/2$ can change the limiting majority outcome while leaving low-order moments similar.

Proposition 3.1. *Under (1),*

$$\mathbb{E}[B_{i1}] = \mathbb{E}[B_{i2}] = \mu := \mathbb{E}[Q], \quad \mathbb{E}[B_{i1}B_{i2}] = \nu := \mathbb{E}[Q^2].$$

For $0 < \mu < 1$,

$$\rho = \text{Corr}(B_{i1}, B_{i2}) = \frac{\nu - \mu^2}{\mu(1 - \mu)} \in [0, 1]. \quad (4)$$

The feasible set is exactly

$$0 \leq \mu \leq 1, \quad \mu^2 \leq \nu \leq \mu. \quad (5)$$

The proof, including exact attainability of the feasible set, is in Appendix A.2.

The pair distribution gives the operational meaning of the moments:

$$\mathbb{P}(B_{i1} = 1, B_{i2} = 1) = \nu, \quad \mathbb{P}(B_{i1} \neq B_{i2}) = 2(\mu - \nu), \quad \mathbb{P}(B_{i1} = 0, B_{i2} = 0) = 1 - 2\mu + \nu. \quad (6)$$

These three probabilities are what a two-call validation set directly observes. They reduce a seemingly many-call question to a pair experiment: ν is the probability that two independent calls on the same example are jointly correct, $1 - 2\mu + \nu$ is the probability that they are jointly wrong, and $2(\mu - \nu)$ is the probability that the two calls disagree. The disagreement probability equals $2\mathbb{E}[Q(1 - Q)]$, so it measures the conditional randomness that voting can average away. The covariance term $\nu - \mu^2 = \text{Var}(Q)$ measures across-example heterogeneity, i.e., how much correctness is locked to the example itself. The normalized version ρ is therefore a same-example correctness correlation: large ρ means repeated calls tend to reproduce successes and failures, while small ρ leaves more recoverable call-level randomness. The two calls do not identify the full law of Q , but they fix the pair table and hence the exact two-moment ambiguity class used below; finite-vote information is then extracted by deterministic moment geometry rather than by calling every validation example many times.

After two labeled calls, the identified population object is the two-moment class

$$\mathcal{M}(\mu, \nu) = \left\{ \pi \in \mathcal{P}([0, 1]) : \int q \, d\pi(q) = \mu, \quad \int q^2 \, d\pi(q) = \nu \right\}. \quad (7)$$

All guarantees below hold uniformly over $\pi \in \mathcal{M}(\mu, \nu)$. For the representative budget with $2n + 1$ calls, the sharp two-call planning interval is

$$L_n(\mu, \nu) = \inf_{\pi \in \mathcal{M}(\mu, \nu)} \int P_n(q) \, d\pi(q), \quad U_n(\mu, \nu) = \sup_{\pi \in \mathcal{M}(\mu, \nu)} \int P_n(q) \, d\pi(q). \quad (8)$$

This notation is used throughout: L_n and U_n are identified-set endpoints, while any point curve introduced later is a parametric completion.

4 Sharp two-call certification

A one-call validation set can estimate μ but cannot identify the pair table, same-example correlation, or within-example stochasticity, so it cannot certify a finite-vote gain distribution-free. The exact mean-only three-vote envelope and the two illustrative latent laws behind this failure are recorded in Appendix A.3. The rest of this section shows what the second labeled call adds: the pair table fixes a two-moment class, and that class has sharp finite-vote endpoints.

4.1 Three-support reduction and quadratic dual

The ambiguity class (7) ranges over all probability laws on $[0, 1]$ with two fixed moments. This is a very large infinite-dimensional object: it includes discrete laws with any number of atoms, continuous densities, singular laws, arbitrary mixtures, and arbitrary placement of mass near the decision threshold. A priori, a sharp two-call certificate for V_n would therefore appear to require optimizing over an unmanageable space of latent correctness distributions.

The next theorem is the main two-call reduction. It says that this apparent obstacle is illusory for any fixed finite vote budget: after the even-budget collapse, every sharp endpoint is witnessed by at most three latent example types and certified by a quadratic envelope of the vote polynomial. This is not a discretization heuristic or a parametric approximation; it is the exact geometry of the two-moment ambiguity class.

Theorem 4.1. *For every feasible (μ, ν) and every fixed $n \geq 1$, both extrema in (8) are attained by distributions supported on at most three points in $[0, 1]$. Equivalently, the quadratic dual extrema are attained and*

$$L_n(\mu, \nu) = \max\{a + b\mu + c\nu : a + bq + cq^2 \leq P_n(q) \forall q \in [0, 1]\}, \quad (9)$$

$$U_n(\mu, \nu) = \min\{a + b\mu + c\nu : a + bq + cq^2 \geq P_n(q) \forall q \in [0, 1]\}. \quad (10)$$

Operationally, the theorem says that two calls reduce vote planning to a small, auditable certificate: a worst-case latent distribution with at most three atoms on the primal side, or a global quadratic inequality on the dual side. The atom locations may change with the objective, but the optimization always stays in the same three-atom search space, independent of the vote budget. Moreover, the proof uses only the two moment constraints and applies to any polynomial objective in q ; for example, the largest possible gain from seven votes over three votes is obtained by replacing P_n with $P_3 - P_1$ in the same moment program. The proof and duality argument are in Appendix A.4.

4.2 Closed-form three-vote certification

The dual program above gives sharp endpoints L_n, U_n for every finite majority budget. The smallest deployable majority budget is $n = 1$, i.e., three calls. This case is also algebraically special: $P_1(q) = 3q^2 - 2q^3$, so bounding V_1 amounts to bounding the unobserved third moment $m_3 = \mathbb{E}[Q^3]$ given (μ, ν) . Because three votes is often the first practical test-time expansion beyond a single call, we state this case separately.

Theorem 4.2. *Let $\mu \in (0, 1)$ and $\rho \in [0, 1]$, with $\nu = \mu^2 + \rho\mu(1 - \mu)$. Put $s = \mu(1 - \mu)(1 - \rho)$. Then, with the usual endpoint conventions at $\mu = 0$ and $\mu = 1$,*

$$L_1(\mu, \nu) = \nu + 2\frac{(\mu - \nu)^2}{1 - \mu} = \mu + s\{2\mu(1 - \rho) - 1\}, \quad (11)$$

$$U_1(\mu, \nu) = 3\nu - 2\frac{\nu^2}{\mu} = \mu + s\{2\mu + 2\rho(1 - \mu) - 1\}. \quad (12)$$

Moreover $U_1(\mu, \nu) - L_1(\mu, \nu) = 2\mu(1 - \mu)\rho(1 - \rho) \leq 1/8$, and if $\mu > 1/2$, then $V_1 > \mu$ for every law in $\mathcal{M}(\mu, \nu)$ exactly when $\rho < 1 - 1/(2\mu)$.

The width bound explains why low-vote planning can be tight after two labeled calls, while the improvement condition separates realized voting gains from gains certified uniformly over every law with the observed moments. The proof and the two-point extremizers are in Appendix A.5.

4.3 Infinite-vote endpoint

By (3), the infinite-vote endpoint is the limit of the finite majority-vote curve and equals a threshold functional of the latent law. The same two moments still give sharp endpoints, but the endpoint is intrinsically less stable because it depends on which side of $1/2$ the latent mass lies.

Theorem 4.3. *Let $U_\infty(\mu, \nu) = \sup_{\pi \in \mathcal{M}(\mu, \nu)} V_\infty(\pi)$ and $L_\infty(\mu, \nu) = \inf_{\pi \in \mathcal{M}(\mu, \nu)} V_\infty(\pi)$. Set $G(1/2, 1/4) = 1/2$, and for every other feasible (μ, ν) define*

$$G(\mu, \nu) = \begin{cases} \frac{\nu - \mu^2}{\nu + 1/4 - \mu}, & \mu \leq 1/2, \nu \leq \mu/2, \\ \min\{1, 3\mu - 2\nu\}, & \text{otherwise.} \end{cases} \quad (13)$$

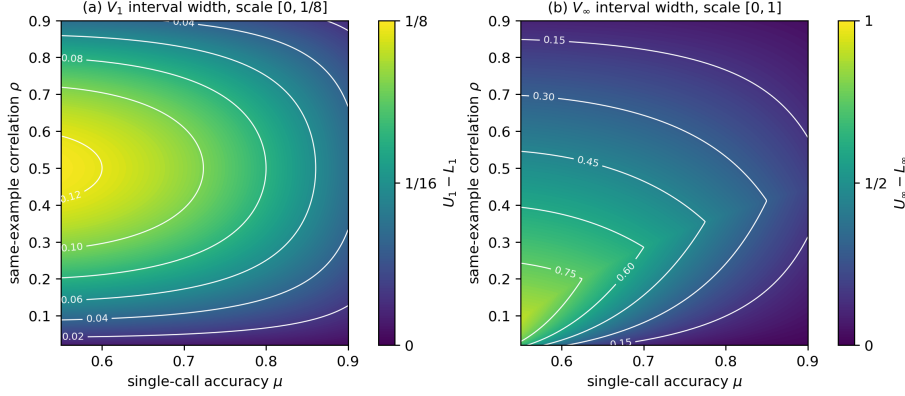


Figure 1: Identified width after two labeled calls. Left: exact width $U_1 - L_1$ for three-vote majority on the sharp scale $[0, 1/8]$. Right: exact width $U_\infty - L_\infty$ for the actual infinite-vote endpoint on $[0, 1]$. Short-horizon planning can be tight while endpoint behavior remains sensitive to mass near $q = 1/2$.

Then $U_\infty(\mu, \nu) = G(\mu, \nu)$ and $L_\infty(\mu, \nu) = 1 - G(1 - \mu, 1 - 2\mu + \nu)$. These values are sharp infima and suprema. Because V_∞ is a discontinuous threshold functional, the extrema need not be attained; on the fractional branch and on parts of the linear branch, sharpness is realized by one-sided feasible sequences.

The endpoint problem is a two-moment tail problem at threshold $1/2$. Unlike fixed finite vote budgets, V_∞ is the discontinuous limit of vote polynomials rather than a polynomial itself, so the sharp interval can remain wide even when three-vote and five-vote intervals are tight. The proof is in Appendix A.6.

Figure 1 summarizes the separation. Three-vote uncertainty is uniformly controlled after two labeled calls, while endpoint uncertainty can remain much larger. The reason is not finite-sample noise but identifiability: finite budgets integrate polynomials of Q , whereas the endpoint reads off which side of the discontinuous threshold $1/2$ the latent mass occupies.

4.4 Projected Wald two-call regions

The population intervals above separate two sources of uncertainty. First, even exact knowledge of (μ, ν) leaves structural uncertainty because many latent laws in $\mathcal{M}(\mu, \nu)$ have the same two-call pair table. Second, a real validation set only estimates (μ, ν) from finitely many examples. The practical certificate should include both effects.

Given N examples with two labeled calls each, set $X_i = ((B_{i1} + B_{i2})/2, B_{i1}B_{i2})$, $\hat{\theta} = (\hat{\mu}, \hat{\nu}) = N^{-1} \sum_i X_i$, and let $\hat{\Sigma}$ be the sample covariance of the X_i 's. For level $1 - \alpha$, use the feasible Wald moment region

$$\mathcal{C}_\alpha = \{\theta \in \mathcal{F} : N(\theta - \hat{\theta})^\top \hat{\Sigma}^\dagger (\theta - \hat{\theta}) \leq \chi_{2,1-\alpha}^2\}, \quad \mathcal{F} = \{(\mu, \nu) : 0 \leq \mu \leq 1, \mu^2 \leq \nu \leq \mu\}, \quad (14)$$

where $\hat{\Sigma}^\dagger$ is interpreted as the inverse or Moore–Penrose inverse as appropriate. The constraint $\theta \in \mathcal{F}$ keeps the projection on feasible population moments; boundary and near-singular cases are handled as described in Appendix B.

For a finite majority budget, project the feasible moment region through the sharp identified intervals,

$$\mathcal{S}_{n,\alpha}^{\text{proj}} = \bigcup_{\theta \in \mathcal{C}_\alpha} [L_n(\theta), U_n(\theta)]. \quad (15)$$

This is the projected identified region. In tables and figures we report its interval hull, the smallest interval containing $\mathcal{S}_{n,\alpha}^{\text{proj}}$. If \mathcal{C}_α contains the true moment pair, then the true population vote accuracy belongs to $\mathcal{S}_{n,\alpha}^{\text{proj}}$ and hence to the reported hull. Because \mathcal{C}_α is a Wald region, this coverage statement has its usual large-sample interpretation. The interval is useful in validation practice because it combines the structural uncertainty caused by observing only two calls per example with the ordinary sampling uncertainty caused by observing only finitely many examples. The same construction is used in the LLM experiments below; numerical details are in Appendix B.

5 Parametric curve completions

The previous section gives unconditional sharp bounds over the full two-moment class. In applications one may also want a single modeled curve rather than an interval at each budget. That requires a parametric completion: a rule that selects one latent law inside the identified set. We study two such completions. The first is maximum entropy, a statistically standard least-committal completion under moment constraints. The second is Latent-difficulty Gaussian-probit (LDGP), an established normal-ogive/probit latent-difficulty model whose two parameters are exactly identified by the two-call moments after scale normalization.

5.1 Maximum-entropy completion

Maximum entropy gives a statistically standard way to choose the least-committal distribution subject to known moment constraints [9]. On the real line, fixing mean and variance selects a Gaussian. On the bounded interval $[0, 1]$, the analogous two-moment maximum-entropy law is not Gaussian; it is a quadratic-exponential density. For an interior feasible pair (μ, ν) , define

$$\psi(\lambda, \kappa) = \log \int_0^1 \exp\{\lambda(q - 1/2) + \kappa(q - 1/2)^2\} dq, \quad (16)$$

with density

$$f_{\lambda, \kappa}(q) = \exp\{\lambda(q - 1/2) + \kappa(q - 1/2)^2 - \psi(\lambda, \kappa)\} \mathbf{1}_{[0,1]}(q). \quad (17)$$

Proposition 5.1. *For every interior feasible (μ, ν) there is a unique (λ, κ) such that (17) has first two moments (μ, ν) . This density uniquely maximizes differential entropy among absolutely continuous laws on $[0, 1]$ with those moments. Equivalently, (λ, κ) uniquely minimizes*

$$J_{\mu, \nu}(\lambda, \kappa) = \psi(\lambda, \kappa) - \lambda(\mu - 1/2) - \kappa(\nu - \mu + 1/4). \quad (18)$$

Moreover,

$$\text{sign}(\lambda) = \text{sign}(\mu - 1/2), \quad \frac{f_{\lambda, \kappa}(q)}{f_{\lambda, \kappa}(1 - q)} = \exp\{2\lambda(q - 1/2)\}.$$

The parameter λ tilts the density across the decision boundary, while κ controls concentration near the center versus the endpoints; the resulting point curve has coordinates $V_n^{\text{ME}} = \int_0^1 P_n(q) f_{\lambda, \kappa}(q) dq$ and $V_\infty^{\text{ME}} = \int_{1/2}^1 f_{\lambda, \kappa}(q) dq$.

5.2 Latent-difficulty Gaussian-probit completion

Latent-difficulty Gaussian-probit (LDGP) gives a complementary completion from the established normal-ogive/probit item-response model for binary correctness [2, 12]. Let $Z \sim N(0, 1)$ be example difficulty and set

$$Q = \Phi(\eta - \gamma Z), \quad \gamma \geq 0, \quad (19)$$

where Φ is the standard normal cdf. The ability parameter η shifts the policy relative to the latent difficulty scale, and γ controls how much example difficulty spreads the success probabilities.

Proposition 5.2. *For every interior feasible pair $0 < \underline{\mu} < 1$, $\underline{\mu}^2 < \nu < \mu$, there is a unique LDGP law of the form (19) matching (μ, ν) . Writing $t = \eta/\sqrt{1 + \gamma^2}$ and $r = \gamma^2/(1 + \gamma^2)$, the parameters are characterized by*

$$\mu = \Phi(t), \quad \nu = \Phi_2(t, t; r),$$

where $\Phi_2(\cdot, \cdot; r)$ is the bivariate standard normal cdf with correlation r . The completed curve is

$$V_n^{\text{LDGP}} = \mathbb{E}[P_n\{\Phi(\eta - \gamma Z)\}], \quad V_\infty^{\text{LDGP}} = \Phi(\eta/\gamma)$$

for $\gamma > 0$. When $\gamma = 0$, the law is constant $Q \equiv \mu$, so the endpoint is 1, $1/2$, or 0 according as $\mu > 1/2$, $\mu = 1/2$, or $\mu < 1/2$.

LDGP is more structural than MaxEnt: it asserts that a one-dimensional difficulty variable and a probit response link explain the heterogeneity in Q , following the standard latent-difficulty interpretation of binary item-response models. Its value here is that the same two-call moments determine the two latent-difficulty parameters, and hence a whole vote curve, under a familiar difficulty model.

ρ	V_1^{ME}	V_2^{ME}	V_∞^{ME}	V_1^{LDGP}	V_2^{LDGP}	V_∞^{LDGP}
0.05	77.15	81.25	97.38	77.23	81.34	96.33
0.20	74.57	76.68	82.64	74.58	76.63	81.99
0.50	72.64	73.52	74.95	71.56	72.08	73.13
0.80	71.35	71.61	71.78	70.23	70.30	70.43

Table 1: Two model-based completions at fixed $\mu = 0.70$. Values are accuracies in percent. Lower same-example correlation corresponds to more recoverable call-level randomness and larger predicted voting gains.

Table 1 illustrates the completions at fixed one-call accuracy. Both MaxEnt and LDGP agree on the qualitative direction: lower same-example correlation produces steeper finite-vote gains. They differ most in high-budget extrapolation, which is expected because the endpoint depends on how each completion distributes mass near $q = 1/2$. In the LLM runs, the nonparametric interval midpoint is the strongest descriptive finite-vote point predictor; LDGP is mildly optimistic relative to the empirical V_1, V_2 values, and MaxEnt is more optimistic still (Appendix E.3).

6 LLM experiments

The experiments use controlled LLM inference in the finite-vote setting. They compare two-call moment regions computed from the first two responses with empirical three- and five-vote accuracies obtained from repeated calls, and they summarize how the observed policies move between stable-error and random-error regimes.

6.1 Protocol and estimands

Each policy is a fixed model, prompt, and decoding configuration; repeated calls differ only through the stochastic decoding seed. We use GLUE QNLI and QQP, cast as yes/no tasks, with 8192 examples per dataset drawn without replacement from the training split. The same examples are used for all models, temperatures, and vote budgets. Experiments run through Ollama’s `/api/generate` endpoint with structured JSON output [15]. The model families are `llama3.1:8b`, `phi4-mini`, and `qwen2.5:7b` [16–18]; temperatures are $T \in \{0.2, 1.0, 2.0\}$ with `top-p = 0.95` and five repeats per example. The JSON parser returned one of the allowed yes/no labels for each recorded response. Appendix C records the exact prompt, seed construction, and other implementation-level protocol details.

For each policy and dataset, the first two repeats estimate $\hat{\mu} = (2N)^{-1} \sum_i (B_{i1} + B_{i2})$, $\hat{\nu} = N^{-1} \sum_i B_{i1} B_{i2}$, and $\hat{\rho} = (\hat{\nu} - \hat{\mu}^2) / \{\hat{\mu}(1 - \hat{\mu})\}$. The structural interval uses only this first-two-call pair table: $\hat{p}_{11} = \hat{\nu}$, $\hat{p}_{10} + \hat{p}_{01} = 2(\hat{\mu} - \hat{\nu})$, and $\hat{p}_{00} = 1 - 2\hat{\mu} + \hat{\nu}$. From $(\hat{\mu}, \hat{\nu})$ we compute the closed-form three-vote interval $[L_1, U_1]$ and a numerical moment-LP interval $[L_2, U_2]$ for five votes. The reported projected regions use the Wald projection in Section 4.4 with $\alpha = 0.05$, so they include both structural two-call uncertainty and moment-estimation uncertainty. Appendix B gives the numerical LP, projection details, and standard-error ranges.

Empirical V_0, V_1, V_2 use all five repeated correctness bits: if example i has c_i correct responses among five, its contribution to an m -vote majority is the hypergeometric probability that a uniformly chosen subset of $m \in \{1, 3, 5\}$ responses has majority correct. Thus the empirical estimates are restricted to the vote budgets directly supported by the five observed responses. In particular, gain columns use this five-repeat empirical V_0 baseline, not the first-two-call moment estimate $\hat{\mu}$.

6.2 Base-policy results

Across all 18 dataset-policy pairs, empirical V_1 lies in the projected 95% region for $[L_1, U_1]$ and empirical V_2 lies in the projected 95% region for $[L_2, U_2]$. The full 18-row table is in Appendix D. The comparison illustrates the role of the two-call moments: they do not recover the full correctness curve, but they give finite-vote regions for the observed three- and five-vote accuracies in this controlled protocol.

Figure 2 shows the contrast from the introduction. High $\hat{\rho}$ corresponds to stable example-level behavior: many examples are effectively fixed successes or fixed failures under the policy, so extra

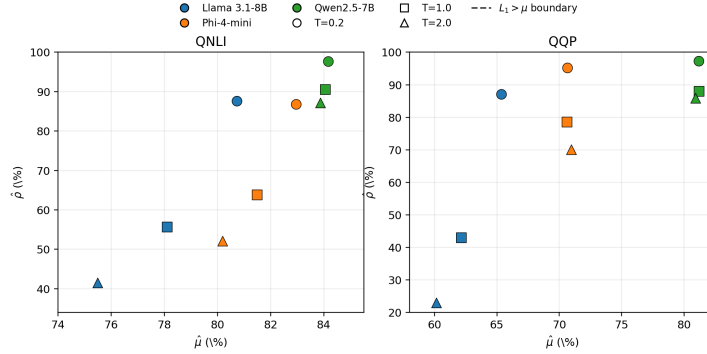


Figure 2: Two-call votability plane. Colors denote model families, markers denote temperatures, and the dashed curve is the sufficient boundary $L_1 > \mu$ for certified three-vote improvement.

calls tend to repeat the first answer. Qwen2.5-7B is the clearest high-accuracy/high-correlation case. It has the highest one-call accuracy in these runs, but its five-vote gains are negligible: at most +0.17 pp on QNLI and +0.04 pp on QQP. This behavior is closer to the stable-error regime than to the random-error regime.

Lower $\hat{\rho}$ corresponds to residual call-level randomness that voting can average. Llama 3.1-8B shows this most clearly as temperature rises. On QQP, moving from $T = 0.2$ to $T = 2.0$ changes $(\hat{\mu}, \hat{\rho})$ from (65.34%, 87.04%) to (60.15%, 22.97%) and changes the five-vote gain from -0.06 pp to $+2.57$ pp. The one-call system becomes less accurate, but it also becomes more votable because the errors become less locked to fixed examples. Phi-4-mini sits between these regimes: on QNLI, higher temperatures reduce correlation enough to create visible vote gains; on QQP, its movement is weaker.

6.3 Policy design consequences

A randomized policy that independently chooses a component protocol on each call is still a conditional-i.i.d. solver after the selector weights are fixed: for each example it induces a latent correctness probability Q_{mix} , and repeated randomized calls are Bernoulli(Q_{mix}). Thus randomization changes the law of Q but not the two-call identification problem. Appendix E reports mixtures that lower same-example correlation and create additional voting gains.

The same distinction produces overtaking: a policy with lower one-call accuracy can beat a stronger one-call baseline after voting when it has lower same-example correlation. Appendix E.2 gives base-policy and randomized-policy examples. No base policy in Figure 2 crosses the worst-case boundary $L_1 > \mu$ after substituting its moments; this boundary is deliberately conservative, so realized gains below it are compatible with adverse latent laws that the first two moments alone cannot exclude.

With five responses per example we validate three- and five-vote regions, not V_∞ . This is consistent with the theory: low-vote regions can be useful even when the endpoint remains sensitive to latent mass near $q = 1/2$.

7 Discussion

The paper separates repeated-inference planning into an identifiable two-call certification component and a parametric completion component. Two labeled calls identify mean accuracy and same-example correctness correlation; those two moments give sharp intervals $[L_n, U_n]$ for any chosen majority-vote budget through its odd representative, three-support primal geometry, and quadratic dual certificates. Point curves such as MaxEnt or LDGP can summarize the remaining ambiguity, but their assumptions must be stated separately from the distribution-free certificate. The empirical results express the same separation operationally. Temperature changes and randomized policies can lower same-example correlation even when one-call accuracy falls, so repeated inference is not ordered by one-call accuracy alone. The two-call statistic distinguishes stable-error policies from policies whose residual call-level randomness can still be converted into finite-vote accuracy by majority voting.

References

- [1] P. Aggarwal, A. Madaan, Y. Yang, and Mausam. Let’s sample step by step: Adaptive-consistency for efficient reasoning and coding with LLMs. In *Proceedings of the 2023 Conference on Empirical Methods in Natural Language Processing*, pages 12375–12396, Singapore, 2023. Association for Computational Linguistics. doi: 10.18653/v1/2023.emnlp-main.761. URL <https://aclanthology.org/2023.emnlp-main.761/>.
- [2] J. H. Albert. Bayesian estimation of normal ogive item response curves using Gibbs sampling. *Journal of Educational Statistics*, 17(3):251–269, 1992. doi: 10.3102/10769986017003251. URL <https://doi.org/10.3102/10769986017003251>.
- [3] B. Atil, S. Aykent, A. Chittams, L. Fu, R. J. Passonneau, E. Radcliffe, G. R. Rajagopal, A. Sloan, T. Tudrej, F. Ture, Z. Wu, L. Xu, and B. Baldwin. Non-determinism of “deterministic” LLM system settings in hosted environments. In *Proceedings of the 5th Workshop on Evaluation and Comparison of NLP Systems*, pages 135–148, Mumbai, India, 2025. Association for Computational Linguistics. doi: 10.18653/v1/2025.eval4nlp-1.12. URL <https://aclanthology.org/2025.eval4nlp-1.12/>.
- [4] D. Bertsimas and I. Popescu. Optimal inequalities in probability theory: A convex optimization approach. *SIAM Journal on Optimization*, 15(3):780–804, 2005. doi: 10.1137/S1052623401399903. URL <https://doi.org/10.1137/S1052623401399903>.
- [5] B. Brown, J. Juravsky, R. S. Ehrlich, R. Clark, Q. V. Le, C. Ré, and A. Mirhoseini. Large language monkeys: Scaling inference compute with repeated sampling. *arXiv preprint arXiv:2407.21787*, 2024. doi: 10.48550/arXiv.2407.21787. URL <https://arxiv.org/abs/2407.21787>.
- [6] M. Chen, J. Tworek, H. Jun, Q. Yuan, H. P. de Oliveira Pinto, J. Kaplan, H. Edwards, Y. Burda, N. Joseph, G. Brockman, A. Ray, R. Puri, G. Krueger, M. Petrov, H. Khlaaf, G. Sastry, P. Mishkin, B. Chan, S. Gray, N. Ryder, M. Pavlov, A. Power, L. Kaiser, M. Bavarian, C. Winter, P. Tillet, F. P. Such, D. Cummings, M. Plappert, F. Chantzis, E. Barnes, A. Herbert-Voss, W. H. Guss, A. Nichol, A. Paino, N. Tezak, J. Tang, I. Babuschkin, S. Balaji, S. Jain, W. Saunders, C. Hesse, A. N. Carr, J. Leike, J. Achiam, V. Misra, E. Morikawa, A. Radford, M. Knight, M. Brundage, M. Murati, K. Mayer, P. Welinder, B. McGrew, D. Amodei, S. McCandlish, I. Sutskever, and W. Zaremba. Evaluating large language models trained on code. *arXiv preprint arXiv:2107.03374*, 2021. doi: 10.48550/arXiv.2107.03374. URL <https://arxiv.org/abs/2107.03374>.
- [7] S. Farquhar, J. Kossen, L. Kuhn, and Y. Gal. Detecting hallucinations in large language models using semantic entropy. *Nature*, 630(8017):625–630, 2024. doi: 10.1038/s41586-024-07421-0. URL <https://doi.org/10.1038/s41586-024-07421-0>.
- [8] R. J. Gallo, M. Baiocchi, T. R. Savage, and J. H. Chen. Establishing best practices in large language model research: An application to repeat prompting. *Journal of the American Medical Informatics Association*, 32(2):386–390, 2025. doi: 10.1093/jamia/ocae294. URL <https://doi.org/10.1093/jamia/ocae294>.
- [9] E. T. Jaynes. Information theory and statistical mechanics. *Physical Review*, 106(4):620–630, 1957. doi: 10.1103/PhysRev.106.620. URL <https://doi.org/10.1103/PhysRev.106.620>.
- [10] S. Karlin and W. J. Studden. *Chebyshev Systems: With Applications in Analysis and Statistics*. Interscience Publishers, New York, 1966.
- [11] L. Kuhn, Y. Gal, and S. Farquhar. Semantic uncertainty: Linguistic invariances for uncertainty estimation in natural language generation. In *International Conference on Learning Representations*, 2023. URL <https://openreview.net/forum?id=VD-AYtP0dve>.
- [12] F. M. Lord. *Applications of Item Response Theory to Practical Testing Problems*. Lawrence Erlbaum Associates, Hillsdale, NJ, 1980.

- [13] P. Manakul, A. Liusie, and M. J. F. Gales. SelfCheckGPT: Zero-resource black-box hallucination detection for generative large language models. In *Proceedings of the 2023 Conference on Empirical Methods in Natural Language Processing*, pages 9004–9017, Singapore, 2023. Association for Computational Linguistics. doi: 10.18653/v1/2023.emnlp-main.557. URL <https://aclanthology.org/2023.emnlp-main.557/>.
- [14] R. Nowak. Estimating the self-consistency of LLMs. *arXiv preprint arXiv:2509.19489*, 2025. doi: 10.48550/arXiv.2509.19489. URL <https://arxiv.org/abs/2509.19489>.
- [15] Ollama. Generate a completion. Documentation, 2026. URL <https://docs.ollama.com/api/generate>. Accessed 2026-05-03.
- [16] Ollama. llama3.1:8b model page. Model documentation, 2026. URL <https://ollama.com/library/llama3.1:8b>. Accessed 2026-05-03.
- [17] Ollama. phi4-mini model page. Model documentation, 2026. URL <https://ollama.com/library/phi4-mini>. Accessed 2026-05-03.
- [18] Ollama. qwen2.5:7b model page. Model documentation, 2026. URL <https://ollama.com/library/qwen2.5:7b>. Accessed 2026-05-03.
- [19] I. Pinelis. On the extreme points of moments sets. *Mathematical Methods of Operations Research*, 83(3):325–349, 2016. doi: 10.1007/s00186-015-0530-0. URL <https://doi.org/10.1007/s00186-015-0530-0>.
- [20] P. Rajpurkar, J. Zhang, K. Lopyrev, and P. Liang. SQuAD: 100,000+ questions for machine comprehension of text. In *Proceedings of the 2016 Conference on Empirical Methods in Natural Language Processing*, pages 2383–2392, Austin, Texas, 2016. Association for Computational Linguistics. doi: 10.18653/v1/D16-1264. URL <https://aclanthology.org/D16-1264/>.
- [21] T. Savage, J. Wang, R. Gallo, A. Boukil, V. Patel, S. A. A. Safavi-Naini, A. Soroush, and J. H. Chen. Large language model uncertainty proxies: Discrimination and calibration for medical diagnosis and treatment. *Journal of the American Medical Informatics Association*, 32(1):139–149, 2025. doi: 10.1093/jamia/ocae254. URL <https://doi.org/10.1093/jamia/ocae254>.
- [22] A. Taubenfeld, T. Sheffer, E. Ofek, A. Feder, A. Goldstein, Z. Gekhman, and G. Yona. Confidence improves self-consistency in LLMs. In *Findings of the Association for Computational Linguistics: ACL 2025*, pages 20090–20111, Vienna, Austria, 2025. Association for Computational Linguistics. doi: 10.18653/v1/2025.findings-acl.1030. URL <https://aclanthology.org/2025.findings-acl.1030/>.
- [23] R. Vashurin, E. Fadeeva, A. Vazhentsev, L. Rvanova, D. Vasilev, A. Tsvigun, S. Petrakov, R. Xing, A. Sadallah, K. Grishchenkov, A. Panchenko, T. Baldwin, P. Nakov, M. Panov, and A. Shelmanov. Benchmarking uncertainty quantification methods for large language models with LM-polygraph. *Transactions of the Association for Computational Linguistics*, 13:220–248, 2025. doi: 10.1162/tacl_a_00737. URL <https://aclanthology.org/2025.tacl-1.11/>.
- [24] A. Wang, A. Singh, J. Michael, F. Hill, O. Levy, and S. R. Bowman. GLUE: A multi-task benchmark and analysis platform for natural language understanding. In *International Conference on Learning Representations*, 2019. URL <https://openreview.net/forum?id=rJ4km2R5t7>.
- [25] X. Wang, J. Wei, D. Schuurmans, Q. V. Le, E. H. Chi, S. Narang, A. Chowdhery, and D. Zhou. Self-consistency improves chain of thought reasoning in language models. In *International Conference on Learning Representations*, 2023. URL <https://openreview.net/forum?id=1PL1NIMMrw>.
- [26] Z. Wang, J. Duan, L. Cheng, Y. Zhang, Q. Wang, X. Shi, K. Xu, H. T. Shen, and X. Zhu. ConU: Conformal uncertainty in large language models with correctness coverage guarantees. In *Findings of the Association for Computational Linguistics: EMNLP 2024*, pages 6886–6898, Miami, Florida, USA, 2024. Association for Computational Linguistics. doi: 10.18653/v1/2024.findings-emnlp.404. URL <https://aclanthology.org/2024.findings-emnlp.404/>.

- [27] G. Winkler. Extreme points of moment sets. *Mathematics of Operations Research*, 13(4): 581–587, 1988. doi: 10.1287/moor.13.4.581. URL <https://doi.org/10.1287/moor.13.4.581>.
- [28] Q. Xiao, D. Bhattacharjya, B. Ganesan, R. Marinescu, K. Mirylenka, N. H. Pham, M. Glass, and J. Lee. The consistency hypothesis in uncertainty quantification for large language models. In *Proceedings of the Forty-First Conference on Uncertainty in Artificial Intelligence*, volume 286 of *Proceedings of Machine Learning Research*, pages 4636–4651. PMLR, 2025. URL <https://proceedings.mlr.press/v286/xiao25a.html>.

A Proofs of main results

This appendix gives formal proofs for the statements whose main-text presentations are abbreviated.

A.1 Even-budget collapse

Let $X \sim \text{Bin}(2n-1, q)$ be the number of correct responses among the first $2n-1$ calls and let $Y \sim \text{Bernoulli}(q)$ be the last call, independent of X . The fair-tie $2n$ -vote success probability is

$$\mathbb{P}(X + Y > n) + \frac{1}{2}\mathbb{P}(X + Y = n).$$

Relative to the odd representative $\mathbb{P}(X \geq n)$, only the boundary events $X = n-1$ and $X = n$ matter. Since

$$q\mathbb{P}(X = n-1) = (1-q)\mathbb{P}(X = n),$$

which follows from $\binom{2n-1}{n-1} = \binom{2n-1}{n}$, the two boundary contributions cancel and the fair-tie $2n$ rule has the same success probability as the $(2n-1)$ -vote strict-majority rule.

A.2 Proof of Proposition 3.1

Conditional on q_i , the two correctness indicators are independent Bernoulli variables with success probability q_i . Therefore

$$\mathbb{E}[B_{i1} | q_i] = q_i, \quad \mathbb{E}[B_{i1}B_{i2} | q_i] = \mathbb{E}[B_{i1} | q_i]\mathbb{E}[B_{i2} | q_i] = q_i^2.$$

Averaging over examples gives $\mathbb{E}B_{i1} = \mu$ and $\mathbb{E}(B_{i1}B_{i2}) = \nu$. Since B_{ij} is binary,

$$\text{Var}(B_{ij}) = \mu(1-\mu), \quad \text{Cov}(B_{i1}, B_{i2}) = \nu - \mu^2,$$

which yields (4) whenever $0 < \mu < 1$.

The feasibility inequalities follow from $0 \leq Q \leq 1$: Jensen's inequality gives $\nu = \mathbb{E}Q^2 \geq (\mathbb{E}Q)^2 = \mu^2$, and $Q^2 \leq Q$ gives $\nu \leq \mu$. Conversely, every pair satisfying $\mu^2 \leq \nu \leq \mu$ is attainable. If $\mu = 0$ or $\mu = 1$, the only possible laws are δ_0 or δ_1 . For $0 < \mu < 1$, the two-point law

$$\pi = (1-p)\delta_0 + p\delta_a, \quad a = \frac{\nu}{\mu}, \quad p = \frac{\mu^2}{\nu},$$

with the limiting interpretation when $\nu = \mu^2$, has mean μ and second moment ν because $a \in [\mu, 1]$ and $p \in [0, 1]$. This proves exact feasibility. Finally, (6) follows from

$$\mathbb{P}(B_{i1} = 1, B_{i2} = 1) = \mathbb{E}Q^2, \quad \mathbb{P}(B_{i1} = 1, B_{i2} = 0) = \mathbb{P}(B_{i1} = 0, B_{i2} = 1) = \mathbb{E}[Q(1-Q)].$$

A.3 Mean-only examples and the one-call envelope

For $\pi_\mu^{\text{det}} = (1-\mu)\delta_0 + \mu\delta_1$, the majority polynomial satisfies $P_n(0) = 0$ and $P_n(1) = 1$, hence $V_n(\pi_\mu^{\text{det}}) = \mu$ for every odd representative. For $\pi_\mu^{\text{hom}} = \delta_\mu$, $V_n(\pi_\mu^{\text{hom}}) = P_n(\mu)$ by definition. The endpoint formula follows by evaluating (3) for these two laws.

For three votes, the mean-only lower and upper ranges are

$$L_1^{\text{one}}(\mu) = \begin{cases} P_1(\mu), & \mu \leq 1/4, \\ (9\mu-1)/8, & \mu \geq 1/4, \end{cases} \quad U_1^{\text{one}}(\mu) = \begin{cases} 9\mu/8, & \mu \leq 3/4, \\ P_1(\mu), & \mu \geq 3/4. \end{cases} \quad (20)$$

Indeed,

$$P_1(q) = 3q^2 - 2q^3, \quad P_1'(q) = 6q(1-q),$$

so the lower convex envelope of P_1 on $[0, 1]$ is $P_1(q)$ on $[0, 1/4]$ and the tangent chord

$$\ell_-(q) = \frac{9q-1}{8}$$

on $[1/4, 1]$. The two pieces match in value and slope at $q = 1/4$, and $\ell_-(1) = P_1(1) = 1$. Jensen's inequality applied to the lower convex envelope gives the lower bound; the linear branch is attained by laws supported on $\{1/4, 1\}$. By the symmetry $P_1(q) = 1 - P_1(1-q)$, the upper concave envelope is $\ell_+(q) = 9q/8$ on $[0, 3/4]$ and $P_1(q)$ on $[3/4, 1]$; the linear branch is attained by laws supported on $\{0, 3/4\}$. This proves the upper formula as well. Since $L_1^{\text{one}}(\mu) \leq \mu$ for every interior μ , one labeled call alone cannot certify three-vote improvement.

A.4 Proof of Theorem 4.1

The moment class (7) is tight and weakly closed on the compact space $[0, 1]$, hence compact. Because P_n is continuous, $\pi \mapsto \int P_n d\pi$ is continuous and linear, so both primal extrema are attained.

An extremizer may be chosen to have at most three support points. The feasible set is a two-moment slice of the probability simplex, and a linear functional attains its maximum and minimum at extreme points of this compact convex slice. Under the three linear constraints $\int 1 d\pi = 1$, $\int q d\pi = \mu$, and $\int q^2 d\pi = \nu$, every extreme point has support size at most three. In the atomic case this is immediate: if four distinct support points q_1, \dots, q_4 carry positive mass, then the four vectors $(1, q_j, q_j^2) \in \mathbb{R}^3$ are linearly dependent, so a nonzero signed perturbation preserves all three moments; small positive and negative perturbation sizes keep the measure nonnegative, contradicting extremality. The general case follows by the same finite-moment extreme-point theorem, equivalently the Winkler–Caratheodory support-size result.

For the quadratic dual, first consider the upper endpoint. Any quadratic $r(q) = a + bq + cq^2$ satisfying $r(q) \geq P_n(q)$ on $[0, 1]$ gives

$$\int P_n(q) d\pi(q) \leq \int r(q) d\pi(q) = a + b\mu + c\nu$$

for every $\pi \in \mathcal{M}(\mu, \nu)$, so the dual majorant value is an upper bound. To see exactness and attainment, consider the compact convex set

$$\mathcal{A}_n = \text{conv}\{(1, q, q^2, P_n(q)) : q \in [0, 1]\} \subset \mathbb{R}^4.$$

Its vertical section at $(1, \mu, \nu)$ is the closed interval $\{(1, \mu, \nu, v) : L_n(\mu, \nu) \leq v \leq U_n(\mu, \nu)\}$. A supporting hyperplane to \mathcal{A}_n at the upper boundary point can be normalized to have last coefficient -1 , giving coefficients (a, b, c) such that $a + bq + cq^2 \geq P_n(q)$ for every q and $a + b\mu + c\nu = U_n(\mu, \nu)$. Thus the dual minimum is attained and equals the primal upper endpoint. Applying the same argument to the lower boundary, or equivalently to $-P_n$, gives an attained quadratic minorant and the formula for L_n .

Nothing in this proof uses a special property of the majority polynomial beyond continuity. Replacing P_n by any continuous function g gives attained extrema of $\int g(q) d\pi(q)$ over $\mathcal{M}(\mu, \nu)$, attained quadratic majorants and minorants, and three-atom primal extremizers. In particular, any polynomial objective, or any linear combination of finite-vote accuracies, is optimized in the same three-atom moment space. Quantities such as the largest possible marginal gain $V_3 - V_1$ are therefore obtained by running the same program with objective $P_3 - P_1$.

A.5 Proof of Theorem 4.2

For three votes,

$$P_1(q) = 3q^2 - 2q^3, \quad V_1 = 3\nu - 2m_3, \quad m_3 := \mathbb{E}Q^3.$$

Thus the upper bound on V_1 is obtained by minimizing m_3 , and the lower bound by maximizing m_3 , under the first two moments.

For any $a \in [0, 1]$,

$$q(q - a)^2 \geq 0.$$

Expanding and integrating gives

$$m_3 - 2a\nu + a^2\mu \geq 0.$$

Choosing $a = \nu/\mu$ for $0 < \mu < 1$ yields

$$m_3 \geq \frac{\nu^2}{\mu}.$$

Equality is attained by a law supported on $\{0, \nu/\mu\}$ with the appropriate weights, so

$$U_1(\mu, \nu) = 3\nu - 2\frac{\nu^2}{\mu}.$$

Similarly,

$$(1 - q)(q - b)^2 \geq 0$$

implies

$$\nu - 2b\mu + b^2 - m_3 + 2b\nu - b^2\mu \geq 0.$$

Choosing $b = (\mu - \nu)/(1 - \mu)$ gives

$$m_3 \leq \nu - \frac{(\mu - \nu)^2}{1 - \mu}.$$

Equality is attained by a law supported on $\{(\mu - \nu)/(1 - \mu), 1\}$, hence

$$L_1(\mu, \nu) = 3\nu - 2 \left\{ \nu - \frac{(\mu - \nu)^2}{1 - \mu} \right\} = \nu + 2 \frac{(\mu - \nu)^2}{1 - \mu}.$$

The endpoint cases $\mu = 0$ and $\mu = 1$ are forced by feasibility.

Substituting $\nu = \mu^2 + \rho\mu(1 - \mu)$ gives the equivalent ρ -form in (11)–(12). Direct subtraction yields

$$U_1 - L_1 = 2\mu(1 - \mu)\rho(1 - \rho) \leq 2 \cdot \frac{1}{4} \cdot \frac{1}{4} = \frac{1}{8}.$$

Finally, for $\mu > 1/2$, uniform improvement over one call is equivalent to $L_1(\mu, \nu) > \mu$. By (11),

$$L_1 - \mu = \mu(1 - \mu)(1 - \rho)\{2\mu(1 - \rho) - 1\}.$$

The prefactor is positive except in the degenerate deterministic case, so strict improvement holds exactly when $2\mu(1 - \rho) > 1$, i.e.,

$$\rho < 1 - \frac{1}{2\mu}.$$

Figure 3 visualizes the certified three-vote gain $\Delta_1^{\text{cert}} = L_1 - \mu$ over the feasible two-call moment region. The zero contour is exactly the theorem's improvement boundary $\rho = 1 - 1/(2\mu)$ for $\mu > 1/2$.

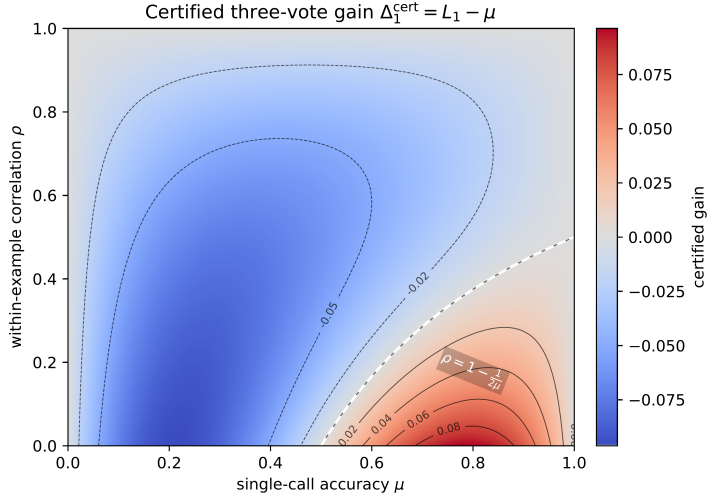


Figure 3: Certified three-vote gain $\Delta_1^{\text{cert}} = L_1 - \mu$ implied by Theorem 4.2. Warm regions certify a uniform gain from three votes over one call; cool regions indicate that no such uniform gain is guaranteed from the two-call moments alone. The dashed white contour is the zero-gain boundary $\rho = 1 - 1/(2\mu)$.

A.6 Proof of Theorem 4.3

Let

$$h(q) = \mathbf{1}\{q > 1/2\} + \frac{1}{2}\mathbf{1}\{q = 1/2\}.$$

The upper endpoint is the supremum of $\int h d\pi$ over $\mathcal{M}(\mu, \nu)$. The exceptional point $(\mu, \nu) = (1/2, 1/4)$ forces $Q \equiv 1/2$, so the value is $1/2$.

For the first nontrivial upper branch, assume $\mu \leq 1/2$ and $\nu \leq \mu/2$. For $a < 1/2$ define

$$\psi_a(q) = \left(\frac{q - a}{1/2 - a} \right)^2.$$

Then $\psi_a(q) \geq h(q)$ on $[0, 1]$: it is nonnegative below the threshold, equals one at the threshold, and is at least one above it. Therefore

$$\int h d\pi \leq \frac{\nu - 2a\mu + a^2}{(1/2 - a)^2}.$$

Minimizing the right side over $a < 1/2$ gives

$$a^* = \frac{\mu/2 - \nu}{1/2 - \mu}$$

and the value

$$\frac{\nu - \mu^2}{\nu + 1/4 - \mu}.$$

Here the denominator is positive away from the exceptional point because

$$\nu + \frac{1}{4} - \mu = (\nu - \mu^2) + (\mu - 1/2)^2.$$

On this branch $a^* \geq 0$ follows from $\nu \leq \mu/2$, and $a^* < 1/2$ follows from $\nu \geq \mu^2$ with equality only at the excluded exceptional point. Thus the optimizing quadratic is admissible. The condition $\nu \leq \mu/2$ is exactly the condition under which the associated two-point Cantelli extremizer has its lower support on the left side of the threshold. If $\nu = \mu^2$, the degenerate law δ_μ is sharp. Otherwise, put $t = 1/2 + \varepsilon$ and

$$x_\varepsilon = \frac{\mu t - \nu}{t - \mu}, \quad p_\varepsilon = \frac{\mu - x_\varepsilon}{t - x_\varepsilon}.$$

For all sufficiently small $\varepsilon > 0$, the branch inequalities give $0 \leq x_\varepsilon < 1/2 < t$ and $0 \leq p_\varepsilon \leq 1$. The two-point law $(1 - p_\varepsilon)\delta_{x_\varepsilon} + p_\varepsilon\delta_t$ matches (μ, ν) , and its endpoint value is p_ε , which tends to $(\nu - \mu^2)/(\nu + 1/4 - \mu)$ as $\varepsilon \downarrow 0$.

For the remaining upper branch, the quadratic

$$\psi_0(q) = 3q - 2q^2$$

satisfies $\psi_0(q) \geq h(q)$ on $[0, 1]$: it is nonnegative on $[0, 1/2)$, equals one at $1/2$, and is at least one on $(1/2, 1]$. Hence

$$\int h d\pi \leq 3\mu - 2\nu,$$

with the trivial additional bound $\int h d\pi \leq 1$. If $3\mu - 2\nu > 1$, a two-point law supported on $\{x, 1\}$ with $x = (\mu - \nu)/(1 - \mu) > 1/2$ attains endpoint value one whenever this branch is active. If $3\mu - 2\nu \leq 1$, set $s = 1/2 + \varepsilon$ and use support $\{0, s, 1\}$ with weights

$$w_s = \frac{\mu - \nu}{s(1 - s)}, \quad w_1 = \frac{\nu - s\mu}{1 - s}, \quad w_0 = 1 - w_s - w_1.$$

They match the two moments. The weights are nonnegative for all sufficiently small $\varepsilon > 0$. Feasibility gives $w_s \geq 0$. On the present branch, either $\mu > 1/2$ or $\nu > \mu/2$, and feasibility gives $\nu/\mu > 1/2$ when $\mu > 0$; hence $w_1 \geq 0$ after taking $s \in (1/2, \nu/\mu)$. Finally,

$$w_0 = \frac{\nu - \mu + s(1 - \mu)}{s}.$$

If $1 - 3\mu + 2\nu > 0$, then $w_0 > 0$ for s close to $1/2$. On the boundary $1 - 3\mu + 2\nu = 0$, this formula gives $w_0 = (1 - \mu)(s - 1/2)/s \geq 0$. Since $s > 1/2$, the endpoint value is $w_s + w_1 = 1 - w_0$, which tends to $3\mu - 2\nu$ as $\varepsilon \downarrow 0$. This proves the stated U_∞ formula.

For the lower endpoint, use the exact symmetry

$$h(q) + h(1 - q) = 1,$$

including at $q = 1/2$, where both terms equal $1/2$. If $\tilde{Q} = 1 - Q$, then

$$\mathbb{E}\tilde{Q} = 1 - \mu, \quad \mathbb{E}\tilde{Q}^2 = 1 - 2\mu + \nu.$$

Therefore

$$L_\infty(\mu, \nu) = 1 - U_\infty(1 - \mu, 1 - 2\mu + \nu),$$

and substituting the upper formula with these reflected moments gives the displayed reflection formula. The same limiting constructions prove sharpness of the lower bound.

A.7 Proof of Proposition 5.1

Let $X = Q - 1/2$. The log-partition function

$$\psi(\lambda, \kappa) = \log \int_{-1/2}^{1/2} e^{\lambda x + \kappa x^2} dx$$

is finite and smooth for all $(\lambda, \kappa) \in \mathbb{R}^2$. Differentiating under the integral sign gives

$$\nabla \psi(\lambda, \kappa) = (\mathbb{E}_{\lambda, \kappa} X, \mathbb{E}_{\lambda, \kappa} X^2),$$

and its Hessian is the covariance matrix of (X, X^2) under the corresponding density. This covariance matrix is positive definite because the curve $x \mapsto (x, x^2)$ is not contained in any affine line on an interval of positive length. Hence ψ is strictly convex.

The convex support of (X, X^2) has interior

$$\{(m, s) : -1/2 < m < 1/2, m^2 < s < 1/4\}.$$

Let the target be $(m, s) = (\mu - 1/2, \nu - \mu + 1/4)$ in this interior. The dual objective $J_{\mu, \nu}(\lambda, \kappa) = \psi(\lambda, \kappa) - \lambda m - \kappa s$ is strictly convex. It is also coercive: along any sequence (λ_j, κ_j) with norm tending to infinity, a subsequential direction u exposes a strictly positive gap between the support function $\sup_x u \cdot (x, x^2)$ and $u \cdot (m, s)$, because (m, s) is an interior point of the convex support. The compact-support Laplace bound for ψ then makes $J_{\mu, \nu}(\lambda_j, \kappa_j) \rightarrow \infty$. Hence $J_{\mu, \nu}$ has a unique minimizer, and its first-order conditions give

$$\mathbb{E}Q = \mu, \quad \mathbb{E}Q^2 = \nu.$$

For entropy optimality, let g be any absolutely continuous density on $[0, 1]$ with the same two moments as $f_{\lambda, \kappa}$. Since $\log f_{\lambda, \kappa}$ is an affine combination of 1 , $q - 1/2$, and $(q - 1/2)^2$, the moment constraints imply

$$H(g) = H(f_{\lambda, \kappa}) - D_{\text{KL}}(g \parallel f_{\lambda, \kappa}).$$

The Kullback–Leibler divergence is nonnegative and vanishes only when $g = f_{\lambda, \kappa}$ almost everywhere, proving uniqueness.

Finally, for $q \in [0, 1]$,

$$\frac{f_{\lambda, \kappa}(q)}{f_{\lambda, \kappa}(1 - q)} = \exp\{2\lambda(q - 1/2)\}.$$

The map $\lambda \mapsto \mathbb{E}_{\lambda, \kappa} Q$ is strictly increasing for fixed κ because its derivative is $\text{Var}_{\lambda, \kappa}(Q) > 0$, and at $\lambda = 0$ the density is symmetric around $1/2$. Hence $\text{sign}(\lambda) = \text{sign}(\mu - 1/2)$.

A.8 Proof of Proposition 5.2

Let Z, E_1, E_2 be independent standard normal variables. Conditional on Z , two independent latent responses from the LDGP model satisfy

$$Q^2 = \mathbb{P}(E_1 \leq \eta - \gamma Z, E_2 \leq \eta - \gamma Z \mid Z).$$

After averaging over Z , this is the probability that the two normal variables $E_1 + \gamma Z$ and $E_2 + \gamma Z$ are both at most η . After standardization, they are bivariate standard normal with common threshold $t = \eta/\sqrt{1 + \gamma^2}$ and correlation $r = \gamma^2/(1 + \gamma^2)$. Hence

$$\mathbb{E}Q = \Phi(t), \quad \mathbb{E}Q^2 = \Phi_2(t, t; r).$$

For a target μ , $t = \Phi^{-1}(\mu)$ is fixed. As r increases from 0 to 1, the bivariate normal cdf $\Phi_2(t, t; r)$ increases continuously from $\Phi(t)^2 = \mu^2$ to $\Phi(t) = \mu$. Strict monotonicity on $(0, 1)$ follows from Plackett's formula

$$\frac{\partial}{\partial r} \Phi_2(t, t; r) = \phi_2(t, t; r) > 0.$$

For an interior feasible ν , there is therefore a unique $r \in (0, 1)$ matching ν , and then $\gamma = \sqrt{r/(1 - r)}$ and $\eta = t/\sqrt{1 - r}$ are unique. The boundary $\nu = \mu^2$ corresponds to $r = 0$ and $\gamma = 0$, while $\nu = \mu$ is the degenerate limit $r \uparrow 1$ and $\gamma \rightarrow \infty$ rather than a finite-parameter interior law. The formula for V_n^{LDGP} is the definition of the completed curve, and the endpoint follows from

$$\mathbb{P}\{\Phi(\eta - \gamma Z) > 1/2\} = \mathbb{P}(\eta - \gamma Z > 0) = \Phi(\eta/\gamma)$$

when $\gamma > 0$. When $\gamma = 0$, $Q \equiv \mu$; applying the definition of V_∞ gives endpoint 1, $1/2$, or 0 according as $\mu > 1/2$, $\mu = 1/2$, or $\mu < 1/2$.

B Computation details

Five-vote moment LP. For five votes,

$$P_2(q) = \mathbb{P}\{\text{Bin}(5, q) \geq 3\} = 10q^3 - 15q^4 + 6q^5.$$

The sharp endpoints are the moment programs

$$L_2(\mu, \nu) = \inf_{\pi \in \mathcal{M}(\mu, \nu)} \int P_2(q) d\pi(q), \quad U_2(\mu, \nu) = \sup_{\pi \in \mathcal{M}(\mu, \nu)} \int P_2(q) d\pi(q).$$

We compute them through the equivalent quadratic-envelope duals

$$U_2(\mu, \nu) = \inf_{a, b, c} \{a + b\mu + c\nu : a + bq + cq^2 \geq P_2(q) \forall q \in [0, 1]\},$$

and analogously for L_2 with the inequality reversed and the objective maximized. The implementation enumerates endpoint and interior contact patterns for the residual polynomial, checks the induced primal weights and moment residuals, and verifies the dual envelope inequality on $[0, 1]$. This gives a deterministic certificate for each reported five-vote endpoint.

Projection of sampling uncertainty. For each dataset-policy pair, the first two calls give independent example-level observations

$$X_i = ((B_{i1} + B_{i2})/2, B_{i1}B_{i2}).$$

Their empirical mean is $(\hat{\mu}, \hat{\nu})$ and their sample covariance gives $\hat{\Sigma}$. The reported 95% regions project $\mathcal{C}_{0.05}$, defined in Section 4.4, through the maps $L_n(\theta)$ and $U_n(\theta)$ and then take the interval hull. The outer two-dimensional optimization is deterministic; boundary points of $\mathcal{F} = \{(\mu, \nu) : 0 \leq \mu \leq 1, \mu^2 \leq \nu \leq \mu\}$ are included explicitly. If $\hat{\Sigma}$ is singular or nearly singular, the implementation uses the Moore–Penrose inverse with a small ridge-equivalent fallback; the feasibility constraint $\theta \in \mathcal{F}$ handles sample means outside the population moment cone. These are row-wise projected moment regions; empirical finite-vote summaries are computed separately from the five recorded correctness bits.

Quantity	Minimum SE (pp)	Median SE (pp)	Maximum SE (pp)
$\hat{\mu}$	0.38	0.42	0.51
$\hat{\nu}$	0.41	0.48	0.55
$\hat{\rho}$	0.33	0.74	1.19

Table 2: Example-level standard-error ranges over the 18 base policy-dataset pairs. The first two rows are obtained from the covariance matrix of $X_i = ((B_{i1} + B_{i2})/2, B_{i1}B_{i2})$; the $\hat{\rho}$ row uses the delta method. With $N = 8192$, the two proportions entering the moment class are estimated at sub-percentage-point scale.

Mixture calculations. Each independently randomized mixture is treated as a fixed new protocol after its selector weights are chosen. It therefore has its own induced latent correctness probability Q_{mix} and is passed through the same two-call moment and vote-interval pipeline as any base protocol. The mixture grid in Appendix E.1 is computed from binary correctness arrays on the same example set. Once the induced binary arrays are fixed, the mixture moments, vote accuracies, and interval calculations are deterministic.

Downstream analysis. The reported tables are computed from binary correctness indicators and the fixed interval routines above. Since the protocol is binary and repeats are sampled independently under a fixed prompt, model, parser, and decoding policy, the estimands are simple averages of correctness indicators. Reruns of stochastic local generation can differ across seeds and software details; the downstream summaries are deterministic once the binary correctness indicators are fixed. The asymptotic confidence calculation uses only the usual sample covariance of the independent example-level vectors X_i .

C Additional experimental protocol details

This appendix records a few implementation-level details of the experimental pipeline. These choices describe the behavior of the released code and are not a conceptual focus of the paper; we include them only to remove ambiguity about the reported results.

C.1 Data preparation and sampling

The final reported experiments use only QNLI and QQP. Both tasks are cast as binary yes/no prediction problems and evaluated by exact label matching. For each dataset, we draw 8192 examples without replacement from the training split and reuse the same draw file across all policies. This same-set design ensures that the two-call estimates $(\hat{\mu}, \hat{\rho})$ and the realized vote accuracies are evaluated on the same question population.

Before writing draw files, the preprocessing script normalizes whitespace and truncates long fields to fixed character caps. For QNLI, the question field is capped at 1200 characters and the sentence field uses the default 3500-character cap. For QQP, both questions are capped at 1200 characters. The reported main experiment uses the draw files

```
qnli_main_8192.jsonl
qqp_main_8192.jsonl
```

produced by the data-preparation script.

C.2 Models and decoding parameters

All model calls are executed locally through Ollama’s `/api/generate` endpoint. The main experiment evaluates three model families:

Family	Ollama tag	Temperatures
Llama 3.1-8B	llama3.1:8b	0.2, 1.0, 2.0
Phi-4-mini	phi4-mini	0.2, 1.0, 2.0
Qwen2.5-7B	qwen2.5:7b	0.2, 1.0, 2.0

All nine policies share the same non-temperature decoding settings:

- `top_p = 0.95`
- `num_predict = 16`
- `stream = false`
- `keep_alive = 30m`
- `request_timeout = 120 seconds`.

The main experiment collects $K = 5$ repeated calls per example. Thus the reported finite-budget quantities are V_0 (one call), V_1 (three votes), and V_2 (five votes).

C.3 Seed construction

The code always passes a deterministic seed to Ollama. For each request, the seed is computed as a stable hash of four pieces of information: the condition seed base, the condition name, the example identifier, and the repeat index. The resulting integer is reduced modulo $2^{31} - 1$ before being sent to the API.

The condition-specific seed bases are:

Condition family	Temperatures	Seed bases
Llama 3.1-8B	0.2, 1.0, 2.0	20263001, 20263002, 20263003
Phi-4-mini	0.2, 1.0, 2.0	20263011, 20263012, 20263013
Qwen2.5-7B	0.2, 1.0, 2.0	20263021, 20263022, 20263023

This choice makes repeated-call experiments reproducible while still ensuring that each condition, example, and repeat uses a distinct stochastic seed.

C.4 Exact prompt templates

The reported main experiment uses `prompt_strategy="direct"`. The fixed instruction prefix is:

Answer the task with Yes or No. Return only valid JSON with key 'answer' and value 'Yes' or 'No'.

For QNLI, the task-specific body is:

Question:
<question>

Sentence:
<sentence>

Does the sentence entail an answer to the question?

For QQP, the task-specific body is:

Question 1:
<question1>

Question 2:
<question2>

Do these two questions ask the same thing?

The full prompt is the concatenation of the instruction prefix, two blank lines, the task-specific body, and a trailing newline. No demonstrations, few-shot examples, or chain-of-thought exemplars are included in the reported main experiment.

C.5 JSON schema and response parsing

Each request asks Ollama to satisfy the following JSON schema:

```
{
  "type": "object",
  "properties": {
    "answer": {
      "type": "string",
      "enum": ["Yes", "No"]
    }
  },
  "required": ["answer"],
  "additionalProperties": false
}
```

The response parser first attempts to decode the raw model output as JSON and read the field `answer`. It maps `Yes` to `True` and `No` to `False`. If JSON parsing fails, the code falls back to a regular-expression search for the tokens `yes` or `no` in the raw output. In the final reported main experiment, however, the valid-answer rate is 100% in all runs, so the fallback path does not affect the reported results in practice.

D Detailed LLM table

Dataset	Policy	$\hat{\mu}$ (%)	$\hat{\rho}$ (%)	$V_1 - V_0$ (pp)	$V_2 - V_0$ (pp)	$[L_1, U_1]_{95}$ (%)	$[L_2, U_2]_{95}$ (%)
QNLI	Llama 3.1-8B $T = 0.2$	80.73	87.64	+0.11	+0.08	[78.10,83.59]	[77.67,83.73]
QNLI	Llama 3.1-8B $T = 1.0$	78.11	55.63	+1.39	+2.03	[74.61,85.17]	[72.92,86.78]
QNLI	Llama 3.1-8B $T = 2.0$	75.49	41.51	+1.62	+2.47	[72.98,84.17]	[71.80,86.99]
QNLI	Phi-4-mini $T = 0.2$	82.96	86.79	+0.11	+0.08	[80.46,85.71]	[80.01,85.85]
QNLI	Phi-4-mini $T = 1.0$	81.49	63.79	+0.94	+1.21	[78.16,87.13]	[76.70,88.02]
QNLI	Phi-4-mini $T = 2.0$	80.19	52.08	+1.34	+1.98	[77.29,87.25]	[75.90,88.84]
QNLI	Qwen2.5-7B $T = 0.2$	84.16	97.66	+0.01	-0.03	[82.87,85.45]	[82.85,85.46]
QNLI	Qwen2.5-7B $T = 1.0$	84.06	90.53	+0.08	+0.17	[81.98,86.25]	[81.73,86.32]
QNLI	Qwen2.5-7B $T = 2.0$	83.86	87.19	+0.05	+0.14	[81.48,86.47]	[81.07,86.60]
QQP	Llama 3.1-8B $T = 0.2$	65.34	87.04	-0.04	-0.06	[61.60,69.27]	[61.02,69.62]
QQP	Llama 3.1-8B $T = 1.0$	62.16	42.97	+1.47	+1.92	[56.90,70.98]	[54.07,74.85]
QQP	Llama 3.1-8B $T = 2.0$	60.15	22.97	+1.73	+2.57	[57.33,68.54]	[55.95,73.17]
QQP	Phi-4-mini $T = 0.2$	70.63	95.17	-0.10	-0.10	[68.46,72.82]	[68.36,72.88]
QQP	Phi-4-mini $T = 1.0$	70.62	78.49	+0.03	-0.02	[66.27,75.69]	[65.04,76.39]
QQP	Phi-4-mini $T = 2.0$	70.95	70.09	+0.12	+0.32	[66.15,77.17]	[64.33,78.39]
QQP	Qwen2.5-7B $T = 0.2$	81.16	97.33	+0.03	+0.02	[79.70,82.61]	[79.67,82.63]
QQP	Qwen2.5-7B $T = 1.0$	81.20	88.00	0.00	-0.01	[78.65,83.96]	[78.24,84.10]
QQP	Qwen2.5-7B $T = 2.0$	80.93	85.88	+0.03	+0.04	[78.16,84.00]	[77.63,84.18]

Table 3: All-temperature repeated-call experiment. V_1 is three-vote majority and V_2 is five-vote majority. The columns $\hat{\mu}$ and $\hat{\rho}$ are first-two-call moment estimates, while gain columns are empirical point gains relative to the five-repeat empirical V_0 baseline. The last two columns project a 95% Wald confidence ellipse for (μ, ν) through the sharp interval maps; empirical V_1 and V_2 are inside their respective projected regions for every row.

E Additional empirical summaries

This appendix reports empirical summaries that use the same binary correctness layer as the main experiment. They are descriptive finite-vote summaries, not additional distribution-free guarantees beyond the two-moment intervals.

E.1 Randomized mixture policies

A randomized policy samples its component independently on each call. After the selector weights are fixed, the mixture is analyzed as a new protocol with its own induced latent correctness probability Q_{mix} , so the same conditional-i.i.d. voting model applies. Table 4 reports mixtures selected for five-vote gain, while Table 5 reports mixtures selected for absolute five-vote accuracy.

Dataset	Type	Mixture	$\hat{\mu}$ (%)	$\hat{\rho}$ (%)	V_2 (%)	$V_2 - \mu$ (pp)
QNLI	pair	0.45·Llama 3.1-8B (T=2.0) + 0.55·Phi-4-mini (T=2.0)	77.91	37.85	81.01	+3.10
QNLI	triple	0.40·Llama 3.1-8B (T=2.0) + 0.40·Phi-4-mini (T=2.0) + 0.20·Qwen2.5-7B (T=2.0)	78.91	38.23	82.35	+3.44
QQP	pair	0.40·Llama 3.1-8B (T=2.0) + 0.60·Qwen2.5-7B (T=0.2)	72.72	42.43	77.89	+5.17
QQP	triple	0.40·Llama 3.1-8B (T=2.0) + 0.10·Phi-4-mini (T=2.0) + 0.50·Qwen2.5-7B (T=0.2)	71.73	39.28	76.76	+5.04

Table 4: Mixtures selected for largest empirical five-vote gain on the auxiliary mixture grid. Each component is selected independently on each call.

Dataset	Type	Mixture	$\hat{\mu}$ (%)	$\hat{\rho}$ (%)	V_2 (%)	$V_2 - \mu$ (pp)
QNLI	pair	0.30·Phi-4-mini (T=0.2) + 0.70·Qwen2.5-7B (T=2.0)	83.60	69.81	84.19	+0.59
QNLI	triple	0.20·Llama 3.1-8B (T=0.2) + 0.30·Phi-4-mini (T=0.2) + 0.50·Qwen2.5-7B (T=2.0)	83.02	60.88	84.39	+1.37
QQP	pair	0.05·Phi-4-mini (T=2.0) + 0.95·Qwen2.5-7B (T=1.0)	80.73	83.86	81.20	+0.47
QQP	triple	0.10·Llama 3.1-8B (T=2.0) + 0.10·Phi-4-mini (T=2.0) + 0.80·Qwen2.5-7B (T=0.2)	78.07	69.85	80.85	+2.78

Table 5: Mixtures selected for largest absolute empirical five-vote accuracy. The best-gain and best-accuracy selections need not coincide.

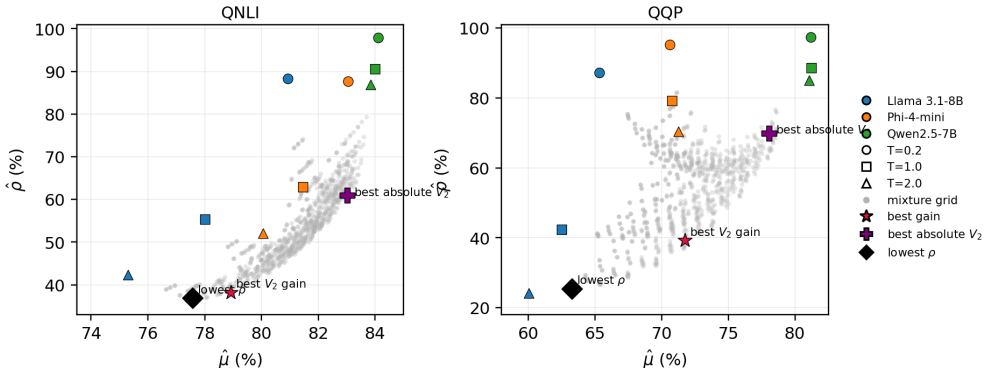


Figure 4: Randomized mixture policies in the two-call votability plane. Grey points are mixture-grid policies; colored markers are base policies. Mixtures can interpolate and sometimes improve the trade-off between one-call accuracy and same-example correlation.

E.2 Overtaking examples

Table 6 gives examples where a lower one-call policy A exceeds a higher one-call comparator B after voting. The differences are paired on the same example set and are reported in percentage points.

Dataset	Policy A	Comparator B	$V_0(A) - V_0(B)$	$V_1(A) - V_1(B)$	$V_2(A) - V_2(B)$
QNLI	Phi-4-mini (T=2.0)	Llama 3.1-8B (T=0.2)	-0.86	+0.37	+1.04
QNLI	0.30·Llama 3.1-8B (T=2.0) + 0.20·Phi-4-mini (T=1.0) + 0.50·Qwen2.5-7B (T=1.0)	Llama 3.1-8B (T=0.2)	-0.04	+1.95	+2.67
QQP	0.40·Llama 3.1-8B (T=2.0) + 0.20·Phi-4-mini (T=2.0) + 0.40·Qwen2.5-7B (T=0.2)	Phi-4-mini (T=1.0)	-0.05	+3.13	+4.56

Table 6: One-call weaker policies can overtake after three- or five-vote aggregation. The phenomenon is explained by lower same-example correlation rather than by one-call accuracy alone.

E.3 Point completions as descriptive summaries

The following table compares three point summaries of the unidentified vote curve against the empirical three- and five-vote estimates in the 18 base-policy runs. These completions are descriptive summaries of an ambiguity class; they are not distribution-free guarantees. In these runs the interval midpoint has the smallest finite-vote error, while LDGP and maximum entropy have positive bias, so the model-based completions are optimistic relative to the empirical vote accuracies.

Target	Point summary	Bias (pp)	MAE (pp)	RMSE (pp)	Max error (pp)
V_1	Interval midpoint	+0.34	0.36	0.61	1.81
V_1	LDGP	+0.48	0.63	0.81	1.78
V_1	maximum entropy	+1.04	1.04	1.19	2.14
V_2	Interval midpoint	+0.22	0.35	0.71	2.20
V_2	LDGP	+0.59	0.78	1.00	2.32
V_2	maximum entropy	+1.22	1.22	1.38	2.52

Table 7: Point-completion errors against empirical finite-vote accuracies. Positive bias means the point completion is optimistic. The interval midpoint has the smallest average error in these runs, LDGP is moderately optimistic, and maximum entropy is more optimistic; this is an empirical diagnostic rather than a theorem.

E.4 A negative movement

QQP with Phi-4-mini $T = 0.2$ has $V_1 - V_0 \approx -0.10$ pp; the recorded example-level comparison gives an interval of $[-0.17, -0.02]$ pp for this adjacent movement. The magnitude is small relative to the positive mixture and temperature effects above, so we treat it as a minor finite-vote observation rather than a separate curve-level phenomenon.

F Existing assets, licenses, and terms of use

Our experiments use existing benchmark datasets, model weights, and local inference software only for research evaluation. We do not redistribute third-party raw data, model weights, or software binaries.

GLUE QNLI and QQP. We use QNLI and QQP from GLUE [24]. GLUE directs users to the original datasets and their terms. QNLI is derived from SQuAD [20], which is distributed under CC BY-SA 4.0. QQP is derived from the Quora Question Pairs release and is subject to the applicable Quora/Kaggle data-use terms. We use these data only for evaluation and do not redistribute raw examples. Relevant pages: <https://huggingface.co/datasets/nyu-ml1/glue>, <https://rajpurkar.github.io/SQuAD-explorer/>, and <https://www.kaggle.com/competitions/quora-question-pairs/rules>.

Models. We use llama3.1:8b, phi4-mini, and qwen2.5:7b through Ollama for local inference. Llama 3.1 is governed by the Llama 3.1 Community License and Acceptable Use Policy; Phi-4-mini is released under the MIT License; Qwen2.5-7B-Instruct is released under Apache-2.0. We do not redistribute any model weights. Relevant pages: https://www.llama.com/llama3_1/license/, <https://huggingface.co/microsoft/Phi-4-mini-instruct>, and <https://huggingface.co/Qwen/Qwen2.5-7B-Instruct>.

Ollama. All generations are run locally through Ollama's `/api/generate` endpoint. Ollama is distributed under the MIT License, and its services are subject to its Terms of Service. Relevant pages: <https://github.com/ollama/ollama/blob/main/LICENSE>, <https://docs.ollama.com/api/generate>, and <https://ollama.com/terms>.

All reported quantities are aggregate correctness and interval summaries.